



PCCP

Tracking the origin of photostability in purine nucleobases: the photophysics of 2-oxopurine

Journal:	<i>Physical Chemistry Chemical Physics</i>
Manuscript ID	CP-ART-02-2019-000879.R2
Article Type:	Paper
Date Submitted by the Author:	30-May-2019
Complete List of Authors:	Martinez-Fernandez, Lara; Universidad Autónoma de Madrid, Chemistry Arslançan, Serra; Universidad Autónoma de Madrid Ivashchenko, Dmytro; Universidad Autónoma de Madrid Crespo-Hernandez, Carlos; Case Western Reserve Univ Corral, Ines; Universidad Autónoma de Madrid, Chemistry

SCHOLARONE™
Manuscripts



Journal Name

ARTICLE

Tracking the origin of photostability in purine nucleobases: the photophysics of 2-oxopurine

Received 00th January 20xx,
Accepted 00th January 20xx

DOI: 10.1039/x0xx00000x

Lara Martínez-Fernández,^a Serra Arslançan,^a Dmytro Ivashchenko^{a,b}, Carlos E. Crespo-Hernández,^c and Inés Corral^{*a,d}

This work scrutinizes the relaxation mechanism of 2-oxopurine. Contrary to its ancestor, purine, which is a UVC chromophore, 2-oxopurine shows a red-shifted absorption spectrum centered in the UVA region. In 2-oxopurine, relaxation along the $\pi\pi^*$ spectroscopic state directs the population from the Franck Condon (FC) region towards a minimum, which acts as a crossroad for the further decay of the system either to triplet states or, alternatively, to the ground state through a C₆-puckered S₁/S₀ funnel. A comparison of the optical properties and excited state potential energy surfaces of purine, 2-oxopurine, 2-aminopurine, 6-oxopurine and adenine, allows establishing how the position and nature of substituent tune the photophysics of purine. For this series, we conclude that both C₂ and C₆ substitution redshift the absorption spectrum of purine, with 2-oxo substitution exhibiting the largest shift. An important exception is the canonical nucleobase adenine, which presents a blue shifted absorption spectrum. The topography of purine's $\pi\pi^*$ potential energy surface experiences major changes when functionalized at the C₆ position. In particular, the disappearance of the minimum along the $\pi\pi^*$ potential energy surface efficiently funnels the excited state population from the FC region to the ground state and increases the photostability of 6-aminopurine (adenine) and 6-oxopurine (hypoxanthine) nucleobases.

Introduction

Nucleic acids belong to the family of macromolecules that are essential to life, and as such their characterization has become a priority, as demonstrated by the number of works devoted to this topic in recent years.¹⁻⁶ Very particularly, and motivated by the connection between DNA photoinduced lesions and cellular damage,⁷⁻¹⁰ many efforts have been devoted to understanding the interaction of DNA with UV light.¹¹⁻¹³ Moreover, understanding the chemical evolution processes undergone by putative prebiotic nucleic acids in early Earth conditions that may have dictated their current composition has also recently awakened strong interest.^{14, 15} DNA chromophores, purine and pyrimidine nucleobases, absorb in the UVB-UVC region and under normal exposure conditions

they are able to dissipate the absorbed energy preserving the macromolecule's integrity.¹⁶⁻¹⁸ The non-radiative decay routes responsible for the remarkable photostability of nucleobases and thus of DNA are now well established. Briefly, the existence of energetically accessible S₁/S₀ decay funnels from the Franck-Condon (FC) region of the initially populated $^1\pi\pi^*$ excited state, allows excited population relaxing efficiently and in ultrafast timescales to the ground state (GS).^{19, 20} However, the specific structural/electronic factors that control the photostability of the canonical purine and pyrimidine nucleobases in comparison to other derivatives are still poorly understood. For instance, the purine chromophore (Scheme 1) has been shown to populate long-lived excited reactive states based on CASPT2/CASSCF calculations and time-resolved spectroscopy, disclosing accessible singlet/triplet crossings and measuring triplet quantum yields of 0.9, respectively.²¹ Substitution of purine with an amino group at either the C₆ or the C₂ positions, forming adenine or 2-aminopurine, respectively, leads to a significant distortion of the potential energy landscape, such that adenine evidences increased photostability while 2-aminopurine exhibits intense fluorescence and non-negligible triplet quantum yield in solution.²²⁻³⁶

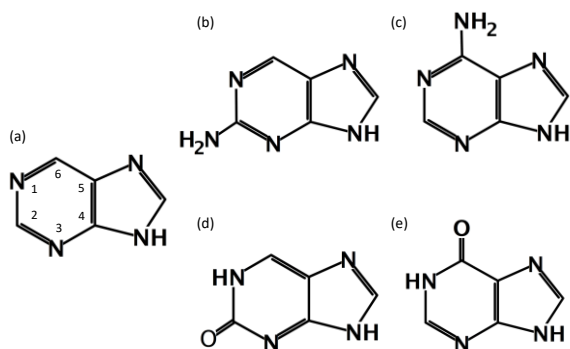
^a Departamento de Química, Universidad Autónoma de Madrid, c/ Francisco Tomás y Valiente 7, 28049 Cantoblanco, Madrid, Spain.

^b Departamento de Química e Bioquímica, Faculdade de Ciências, Universidade do Porto, R. Campo Alegre s/n, , 4169-007 Porto Portugal

^c Department of Chemistry and Center for Chemical Dynamics, Case Western Reserve University, 10900 Euclid Avenue, Cleveland, Ohio 44106, United States.

^d IADCHEM. Institute for Advanced Research in Chemistry, Universidad Autónoma de Madrid, 28049 Cantoblanco, Madrid, Spain

Electronic Supplementary Information (ESI) available: [CASSCF Molecular Orbitals, Absorption spectra in the range 180-400 nm, potential energy profiles' solvent dependence]. See DOI: 10.1039/x0xx00000x



Scheme 1 Scheme including atom labelling of (a) purine chromophore and its amino- and oxo- monosubstituted derivatives (b) 2-aminopurine, (c) adenine, (d) 2-oxopurine and (e) 6-oxopurine.

The incorporation of oxo substituents in the purine chromophore has also been shown to have a strong influence in the topography of its excited state potential energy surface (PES) and in its photophysics. In fact, when this functional group is incorporated at the C6 position (as in 6-oxopurine/hypoxanthine), the PES of purine reshapes leading to a barrierless connection between the FC region of the $\pi\pi^*$ state and a S_1/S_0 funnel that efficiently conducts the population to the GS.³⁷⁻⁴¹ As such, this system is considered to be photostable.³⁷⁻⁴¹

The aim of this work is to decipher the molecular deactivation mechanism of 2-oxopurine based on the mapping of its excited state singlet and triplet PESs with complementary theoretical approaches to establish for the first time the connection between the substituent's nature and position, and the intrinsic photophysics of purine nucleobases.

Computational Details

The GS equilibrium geometry of 2-oxopurine was optimized at the CASSCF/6-31G(d,p) level of theory.⁴²⁻⁴⁴ The (14,11) active space employed consists of the complete π system plus the lone pair of the carbonyl group, see Figure S1. Using this geometry as a reference, the first absorption band of the spectrum of 2-oxopurine was modelled considering the MS-CASPT2/SA5-CASSCF(14,11)/6-31G(d,p) protocol⁴⁵ and two different IPEA shifts 0.0 and 0.25 au,⁴⁶ (Table 1 and S1). The absorption spectrum up to 180 nm (6.9 eV), in Figure S2, was computed at the MS-CASPT2/SA14-CASSCF(14,11)/6-31G(d,p) level of theory. To unravel the photophysics of this system, starting from the FC region we have mapped the topography of the excited PES relevant to the deactivation of this system calculating the minimum energy paths (MEPs) from the spectroscopic state, S_1 . To this purpose, we have resorted to the CASSCF method with the same active space described above and considering two roots. The minimum found along MEP was reoptimized at the SA2-CASSCF(14,11)/6-31G(d,p) level of theory. This was the same level of theory employed for the location of the funnel for the deactivation to the GS and the singlet-triplet crossing. Final energies for the stationary points and interstate funnels along the deactivation potential

energy profile were computed with the CASPT2 method and considering 3 roots.

For calculating the density difference between the ground and excited states of the other purine derivatives, (Figure S3) we employed perturbatively modified CASSCF wave functions considering the following active spaces and number of roots: 2-aminopurine (12,11)/SA(3), adenine (12,10)/SA(5), hypoxanthine (12,10)/SA(3) and purine (16,19)/SA(3). The 6-31G(d) basis set was considered for these calculations.

The absorption spectrum and the topography of the PES were also investigated using two additional computational protocols, namely DFT, considering the M062X functional,⁴⁷ and the algebraic diagrammatic construction scheme of the polarization propagator in its second order, ADC(2),⁴⁸ combined with the triple- ζ quality basis sets of Dunning and Alrichs, cc-pVTZ⁴⁹ and def-TZVP,⁵⁰ respectively (Figure 1, Figure S2 and Table S1). In the framework of DFT, we have also estimated the effect of water and other solvent continua (using the Polarizable Continuum Model)^{51, 52} in the absorption spectrum and the geometries of the S_1 minimum and conical intersections. (Figure 2 and S4). For this, we have considered the linear response (LR) version of PCM, for which excited state analytical gradients are available.⁵³ Additionally for water, State Specific (SS-PCM) single point calculations were also performed (Figure S4).^{54, 55} For the location of conical intersections with ADC(2), we have employed the algorithm implemented by Levine et al. avoiding the use of non-adiabatic coupling.⁵⁶ Spin-Orbit couplings were estimated using the single particle Breit-Pauli operator with an effective charge approximation as implemented in the PySOC code⁵⁷ which was interfaced with Gaussian09. All the multiconfigurational calculations were performed with MOLCAS software (version 8),⁵⁸ whilst ADC(2) and DFT calculations were carried out with Turbomole⁵⁹ and Gaussian09.⁶⁰

Results

Absorption spectra

The absorption spectrum of 2-oxopurine calculated at the CASPT2 level of theory shows two bands peaking at 321 nm and 239 nm, the first 8 times more intense than the second (Table 1 and Figure 1), followed by a very intense absorption beyond 200 nm, (Figure S2). Despite underestimating the intensity of the second band, our calculations predict the transitions energies in excellent agreement with the experiment of Czochralska et al. recorded in aqueous buffered solution (315 nm and 238, with ϵ 4.9 $\cdot 10^3$ and 2.9 $\cdot 10^3$).^{61, 62} These 2 transitions showing $\pi\pi^*$ character are followed by almost dark $n\pi^*$ absorptions, S_2 and S_4 , transferring density from the carbonyl group to the π heterocycle cloud of the nucleobase. The computed CASPT2 energies for the $\pi\pi^*$ states are in line with the values provided by the second order, MRMP2,⁶³ ADC(2) and CC2, particularly for the lowest and brightest state, the energy difference being smaller than 0.2

eV for all the methods (Table S1). Although the active space selected for the reference CASSCF calculations (Figure S1) does not include the N_3 lone pair participating in the $n\pi^*$ transitions according to the monoconfigurational methods, the energy gap between the mono and multireference approaches calculated for these transitions was found to be only slightly larger (ca. 0.4-0.5 eV). When comparing CASPT2 with DFT, we observe that although still underestimated, the DFT energies for the $n\pi^*$ states are closer (average deviation 0.25 eV) to CASPT2 but the $\pi\pi^*$ excited states are shifted to higher energies. The incorporation of bulk water solute interactions was found to affect more significantly the $n\pi^*$ transitions, which are shifted by 0.3 eV to the blue, whilst the first $\pi\pi^*$ state (S_1) destabilizes by ca. 0.1 eV and the S_3 remains almost unaffected (Figure 1 and S1). These shifts are in line with the CASSCF gas phase calculated dipole shown in Table S1. The greater dipole moment of the GS compared to the rest of electronically excited state is expected to more strongly stabilize the S_0 in polar environments, producing, thus, a shift to the blue for all the electronic states considered except for the S_3 , which presents a comparable dipole moment to the S_0 .

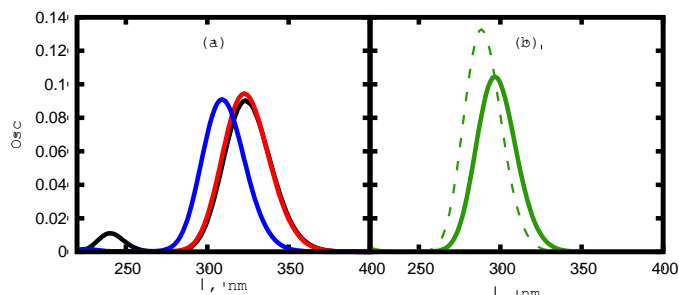


Figure 1 Gas phase simulated absorption spectra for 2-oxopurine computed at the (a) CASPT2 (black), ADC(2) (red), CC2 (blue) levels of theory and (b) at the TD-M062X level of theory in gas phase (solid green) and water (dashed green). A total number of 4 excited states have been considered in the simulations.

In order to estimate the potential role of the triplets in the deactivation mechanism of 2-oxopurine, we have computed the energy of the lowest-lying triplets at relevant regions of the PES. At the FC region, CASPT2 finds the three lowest triplets, T_1 , T_2 and T_3 , all of them showing $\pi\pi^*$ character, separated by ca. 1 eV from the lowest lying bright state (Table 2).

Table 1. MS-CASPT2 main configurations, weights, energies (in nm and eV) and oscillator strength for the lower lying singlet excited states of 2-oxopurine.

	Main Configurations	Weights	Energies (nm)	Energies (eV)	f
MS-CASPT2					
S_1	$\pi_1\pi_2^{\text{H}}\text{H}$	0.75	321	3.86	0.0903
S_2	$n_0\pi_1^{\text{H}}\text{H}$	0.78	249	4.97	0.0004
S_3	$\pi_2\pi_1^{\text{H}}\text{H}$	0.44	239	5.20	0.0109
S_4	$\pi_1\pi_2^{\text{H}}\text{H}$	0.12	202	6.13	0.0001

The calculations of the triplet energies at CC2, and ADC(2) levels follow very much the CASPT2 scenario with the lowest-lying triplet states lying 1 eV either above or below the

spectroscopic state (Table S2). TD-DFT (TD-DFT-PCM), however, finds a $n\pi^*$ triplet lying only 0.2 (0.4) eV above the S_1 .

Table 2. MS-CASPT2 energies (in nm and eV) for the lowest lying triplet excited states of 2-oxopurine.

	Main Configurations	Energies (nm)	Energies (eV)
MS-CASPT2			
T_1	$\pi_1\pi_2^{\text{H}}\text{H}$	466	2.66
T_2	$\pi_1\pi_1^{\text{H}}\text{H}$	263	4.71
T_3	$\pi_2\pi_2^{\text{H}}\text{H}$	259	4.79

Potential Energy Surfaces

A schematic potential energy profile along the coordinates relevant to the deactivation of 2-oxopurine is shown in Figure 2. Note that the small differences in the relative energies compared to Table 1 are due to the number of states considered for the calculation of the absorption spectrum and the deactivation profiles. The MEP along the most stable and brightest state, S_1 , starting from the FC region leads directly and in a barrierless manner to a minimum in this potential, $S_{1\text{min}}$ (Figure S5), which lies 3.40 eV above the GS minimum, $S_{0\text{min}}$, at MS-CASPT2/CASSCF level of theory (Figure 2). This corresponds to a stabilization of ~ 0.4 eV with respect to the vertical excitation value calculated at the same level of theory. Although 0.5 eV higher in energy, the gas phase energy of this minimum is in line with the fluorescence emission registered in water for the corresponding nucleoside, 2'-deoxyisinosine.⁶⁴ Consistently with the character of the transition, reaching this minimum significantly redistributes the electron density along the pyrimidine ring. In particular, we observe the stretching of the $C_2\text{-O}$ and $N_3\text{-C}_4$ bonds, whilst the $C_2\text{-N}_3$ bond experiences reinforcement (see Figure 3 and recall Scheme 1 for atom numbering). The $C_5\text{-C}_6$ and $N_1\text{-C}_6$ bond distances also undergo a weakening, although to a smaller extent. Accessing the S_1/S_0 funnel, responsible for mediating the decay to the GS, requires the further stretching of the $C_2\text{-O}$ and $N_3\text{-C}_4$ bonds, simultaneous with the puckering of C_6 atom and the tilting of the H atom lying at the same C center. This S_1/S_0 funnel was located 4.03 eV above the S_0 equilibrium geometry, i.e., 0.6 and 0.2 eV above the $S_{1\text{min}}$ and the vertical energy of the S_1 at the FC region, respectively.

The ADC(2) method delivers a qualitatively similar PES for the S_1 . The ADC(2) optimized geometry for $S_{1\text{min}}$ is very similar to that predicted by CASPT2, although more stable; that is 2.71 eV relative to the $S_{0\text{min}}$. Interestingly, the main difference between the two computed geometries is a moderate out-of-plane distortion of the $C_6\text{-H}$ moiety, very much reminiscent of the MS-CASPT2 S_1/S_0 conical intersection structure and geometry predicted by ADC(2) method for this crossing, which additionally shows the subtle out-of-plane deviation of other atoms of the pyrimidine ring, such as N_1 . This similarity would also justify the planar topography of the ADC(2) PES connecting the $S_{1\text{min}}$ and the S_1/S_0 funnel, only separated in

this case by 0.1 eV. It is, however, well-known the propensity of the ADC(2) approach to fail to accurately describe the topography of the PES around S_1/S_0 funnels.⁶⁵ DFT predicts the least stable $S_{1\text{min}}$ of all the methods considered, lying 0.3 eV below the S_1 FC energy and 3.90 eV above the $S_{0\text{min}}$, consistent with a structure of the minimum closer to the FC geometry, although showing the same ring deformations as described for the CASSCF minimum. Similarly to ADC(2), DFT computes the S_1/S_0 funnel at 0.06 eV above the $S_{1\text{min}}$. The DFT S_1/S_0 crossing geometry resembles very much ADC(2)'s, but with a much greater distortion of the pyrimidine ring, especially of the N_1 atom. The potential energy profile delivered by the TD-DFT/PCM is almost identical to the one obtained in the gas phase, independently of the solvent polarity and the solvation model considered, i.e. LR or SS (Figure S4).

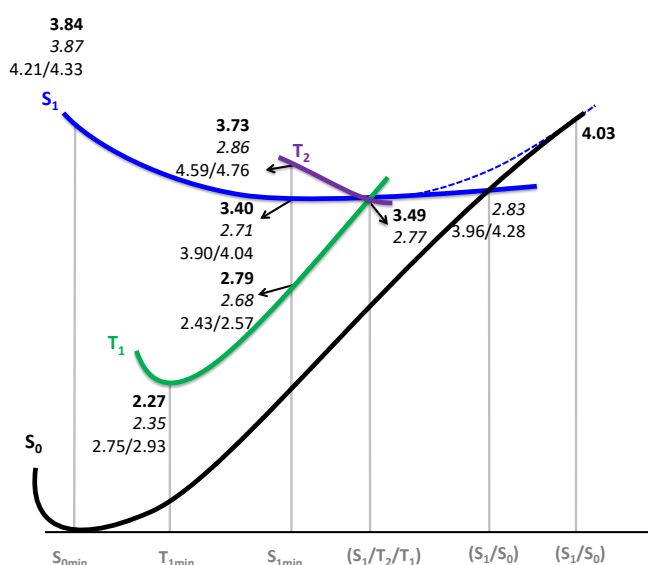


Figure 2 Singlet and triplet potential energy profiles relevant to the decay mechanism of 2-oxopurine. Energies in eV, relative to the ground state equilibrium geometry, calculated at the MS-CASPT2 (bold), ADC(2) (italics) and M062X/PCM-M062X (plane) levels of theory.

We now shift the focus to discuss the potential transfer of population to the triplet states while the population is visiting the $S_{1\text{min}}$. To this purpose, we have computed the energies of the triplets at the $S_{1\text{min}}$, with all the methods considered in this study. Furthermore, we have estimated the coupling of the S_1 with the closest triplets both at CASPT2 and TD-DFT levels of theory. Interestingly, both CASPT2/CASSCF and ADC(2) approximations predict energetically close triplets at $S_{1\text{min}}$ (See Figure 2). In particular, CASPT2 predicts T_2 only 0.3 eV above $S_{1\text{min}}$, and the T_1 lying 0.6 eV below, in agreement with RI-CC2/aug-cc-pVDZ calculations.⁶⁶ In the case of ADC(2), both the T_1 ($n_o\pi_1^*$) and T_2 ($\pi_1\pi_1^*$) lie close to the $S_{1\text{min}}$, the energy gaps being 0.03 and 0.15 eV, respectively. In fact, we were able to optimize a $S_1/T_1/T_2$ crossing in the vicinity of the $S_{1\text{min}}$, ($E_{\text{CASPT2}} = 3.49$ eV, $E_{\text{ADC(2)}} = 2.77$ eV) both structures differing in the $C_2\text{-O}$, and the pair of $C_2\text{-N}_3$ and $C_4\text{-C}_5$ bond distances, which respectively stretch and reinforce when moving from the minimum to the $S_1/T_1/T_2$ crossing. DFT, however, predicts

larger energy gaps, independently of the environment. In fact, T_2 ($n_o\pi_1^*$ in the gas phase and $\pi_1\pi_2^*$ in water continuum) is separated by 0.7 eV from the minimum and the gap for the T_1 is even larger (see Figure 2). Consistently with the character and the energy gaps found with MS-CASPT2 and DFT, we calculate, at the $S_{1\text{min}}$, SOCs with the T_2 state that amount to 62 and 4 cm^{-1} , respectively.

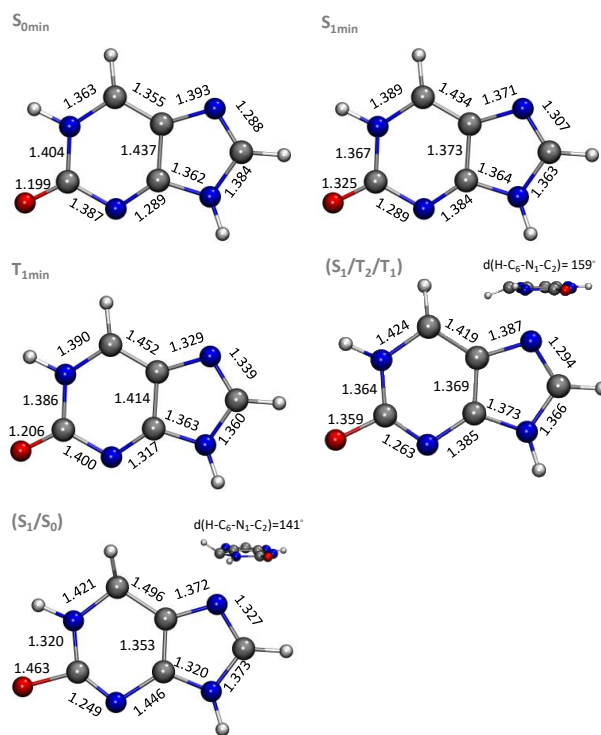


Figure 3 Most relevant CASSCF optimized geometries along the Potential Energy Surface of 2-oxopurine. Distances in Å.

Discussion

Now we discuss how the topography of purine's PES is affected by the position and nature of the substituent. As highlighted above, this has important implications for understanding which is the origin of the photostability of nucleobases, (Figure 4 and Scheme 2). To fill this gap in knowledge, we compare the features of the PES computed for 2-oxopurine with those of the purine chromophore, adenine, 2-aminopurine, and 6-oxopurine, reported in other works. In particular, we focus on the shape of the PES corresponding to the first bright electronic state, which qualitatively leads to the same reorganization of the electronic density in all these nucleobases (see Figure S3).

The first important difference between 2-oxopurine and purine is already observed in the absorption spectrum.²¹ Importantly, introducing a carbonyl group at position 2 of the purine chromophore stabilizes the $\pi\pi^*$ excited state by ca. 0.9 eV, whilst destabilizes almost to the same extent the lowest $n\pi^*$ transition, as already concluded in previous studies.⁴¹ This

leads to an inversion of the state ordering, while the spectroscopic $\pi\pi^*$ excited state is the S_2 in the case of purine, this state becomes the S_1 in 2-oxopurine. Similarly to 2-oxopurine, the S_2 $\pi\pi^*$ PES of purine is characterized by the presence of a minimum, moderately coupled with triplet states (SOC 14 cm^{-1}), which after crossing the ${}^1n\pi^*$ state, reaches a $S_1(\pi\pi^*)/S_0$ degeneracy region (see Figure 4). This conical intersection, although showing out-of-plane distortion of the pyrimidine ring, differs from the one optimized for 2-oxopurine in the atom deviating from the plane, whilst $S_1(\pi\pi^*)/S_0$ -CI is characterized by a C_2 puckering in purine, C_6 puckering was observed in the oxo nucleobase. Also importantly, despite the energy of this crossing lies below the entrance channel in purine, the barrier separating the $S_{2\text{min}}$ and the $S_1(\pi\pi^*)/S_0$ -CI, which is not present in the oxo substituted nucleobase, diverts the population towards more energetically accessible channels. In fact, the population reaching the S_2 in purine initially decays to a planar S_1 $n\pi^*$ minimum where it gets trapped (Figure 4).

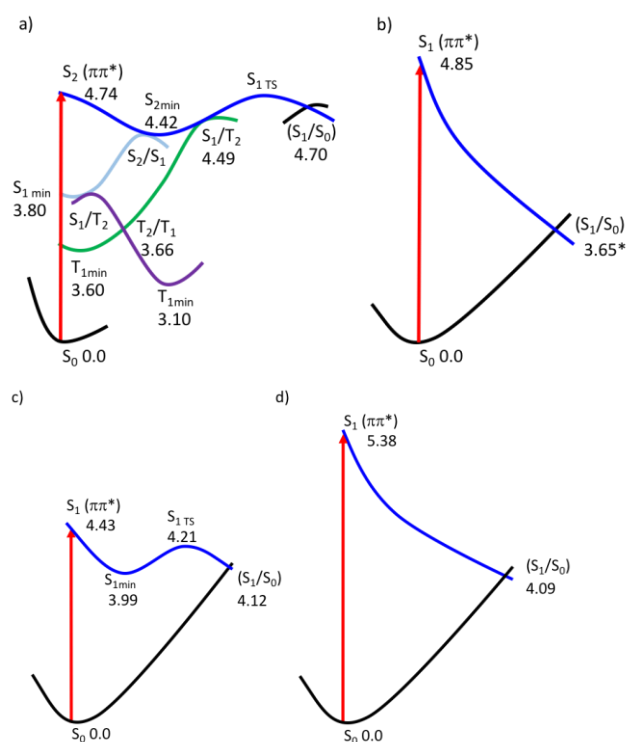


Figure 4 Main features of the potential energy surfaces relevant to the deactivation routes from the optical electronic states in purine (a), hypoxanthine (b), 2-aminopurine (c) and adenine (d) adapted from Refs [21], [37] and [22], respectively. * MRMP2 energy for the conical intersection was taken as the mean value of S_1 and S_0 states.

It is important to note, that $n\pi^*$ transitions in purine involve the lone pair of N_3 of the purine chromophore, whilst in the case of 2-oxopurine, the lone pair is localized at least partially in the carbonyl group. Similarly to 2-oxopurine, purine $S_{1\text{min}}$ acts as a doorway for the transfer of population to the triplet manifold, due to the non-negligible SOC (18 cm^{-1}) calculated at

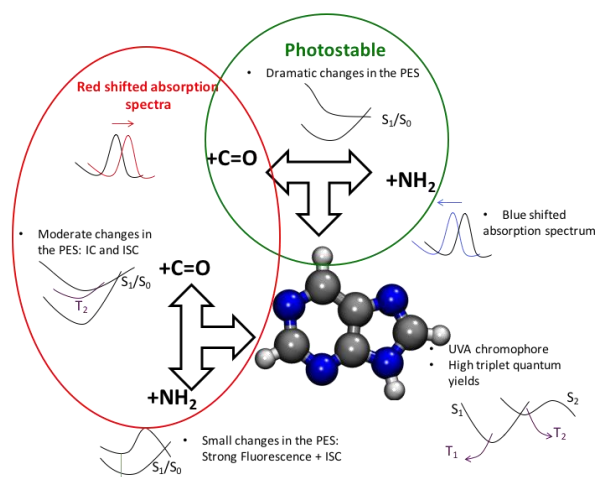
this region of the PES and the important energetic separation between the minimum position and the $S_1(n\pi^*)/S_0$ funnel (0.6 eV), puckered at the C_6 position (Figure 4). This translates into a triplet quantum yield of 0.88 and an almost negligible fluorescence quantum yield in purine nucleobase.²¹ It is remarkable that even though these two systems contain only atoms from the 1st and 2nd period, the SOC registered for 2-oxopurine are unusually large (62 cm^{-1}).

We discuss next how the nature of the substituent and its position affects the photophysics of purine. To fulfill this goal, we compare the optical properties and photophysics of 2-aminopurine, 6-oxopurine and 6-aminopurine (adenine) with our results. In the case of 2-aminopurine, we take as reference the work of Serrano-Andrés,²² which employed the closest theoretical protocol to the one considered in the present study (MS-CASPT2/CASSCF gas phase calculations without symmetry constraints), whilst we select the work of Villabona-Monsalve³⁷ for the case of 6-oxopurine (see Figure 4).

The substitution of the purine heterocycle in position 2, no matter if it is with an amino or with an oxo substituent, seem to have the same effect over the lowest lying excited states, see discussion below. Similarly to 2-oxopurine, the incorporation of an amino substituent at position 2, leads to the stabilization of the lowest $\pi\pi^*$ excitation and the destabilization of the lowest $n\pi^*$ transition compared to purine, although these shifts are much less pronounced in the amino compound (0.3-0.4 eV).²² As in purine and 2-oxopurine, the PES for the spectroscopic state of 2-aminopurine delineates a minimum of planar geometry, which converges into a $S_1(\pi\pi^*)/S_0$ decay funnel with the GS.²² Similarly to purine, this crossing presents a C_2 puckered structure (with an out-of-plane deviation from the NH_2) and an energy barrier was found to separate the minimum and S_1/S_0 crossing, revealing that amino substitution in position 2 has a more moderate effect both in the optical properties and the shape of the excited state PES than the oxo-substituent. The trapping of the population in the $S_1(\pi\pi^*)$ minimum favors emission in this system. In fact, 2-aminopurine is highly fluorescent ($\phi_F=0.68$) in aqueous buffer solution.²⁸ However, the high triplet yield recorded for 2-aminopurine in acetonitrile ($\phi_T=0.4$)²⁸ also suggests the existence of strongly coupled triplets in the vicinity of the $S_{1\text{min}}$, comparable to unsubstituted purine and 2-oxopurine.

The influence of the substituent position in the photophysics of these systems is analyzed by comparison of the absorption spectra and excited state PESs of 2-oxopurine and hypoxanthine. Likewise the other two substituted purines examined, hypoxanthine presents a stabilized $\pi\pi^*$ spectroscopic state (0.25 eV), whilst the $n\pi^*$ excited state is severely destabilized (1.1 eV).³⁷ Interestingly, substitution at position 6 of the purine ring with an oxo functional group has the greatest effect over the rest of substitution scenarios considered, especially in what concerns the shape of the excited state PES. Very interestingly, in contrast to the other 3 systems examined, the PES for the spectroscopic $\pi\pi^*$ state presents no minimum, but the FC is directly connected with

the $S_1(\pi\pi^*)/S_0$ funnel, characterized by the C_2 - N_3 out-of-plane deviation.



Scheme 2 Summary of the main effects observed on the absorption spectrum and photophysics of purine base upon introducing NH_2 or $C=O$ groups at C_2 or C_6 positions.

Amino functionalization at C_6 position of purine was found to have the same net effect on the topography of the PES as C_6 oxo substitution. However, unlike the other purine derivatives analyzed, a shift of the absorption spectrum to higher energies was predicted for adenine taking purine as a reference.²²

Conclusions

In conclusion, we studied the optical properties and potential energy surfaces of 2-oxopurine with state of the art computational methods. Our results show that the absorption spectrum of 2-oxopurine is centered in the UVA region (326 nm, 3.8 eV) and reveal the existence of a planar minimum separated by some tenths of eV from the funnel redirecting the population to the GS. Interestingly, our calculations detect the presence of strongly coupled triplets at the position of the S_{1min} , whose population is predicted to compete with internal conversion along the singlet manifold. Comparing the optical properties and photophysics of 2-oxopurine presented in this work with those of purine, adenine, 2-aminopurine, and hypoxanthine, we conclude that:

* both amino and oxo substitution at position 2 of the purine chromophore shifts to lower energies the absorption spectrum of purine, with oxo substitution having a larger effect than the amino group in the stabilization of the absorption energy.

* C_6 substitution, however, leads to opposite effects on the absorption spectrum depending on the nature of the substituent. Whilst the amino group produces a shift to higher energies of the spectroscopic state, substitution with an oxo group lowers the energy of the brightest $\pi\pi^*$ excited state.

the effect that substitution plays on the topography of the spectroscopic PES follows, however, a different trend. Substitution at C_2 position (oxo or amino) broadly maintains the features of the spectroscopic $\pi\pi^$ PES of purine, i.e.,

deactivation from the FC leads to a minimum strongly coupled to a neighbor triplet state. Importantly, whilst the amino substituent conserves the transition state separating the minimum and the GS funnel found in purine, the incorporation of the oxo substituent at the same position eliminates the barrier. Functionalization at C_6 position, independent of whether oxo or amino substituents are employed, has a major impact in the shape of the PESs, which show no minimum, and this translates into photostable systems.

Acknowledgments

This work has been supported by the Project PGC2018-094644-B-C21 of the Ministerio de Economía y Competitividad of Spain. I.C. and L.M.F gratefully acknowledge the “Ramón y Cajal” and “Juan de la Cierva-Incorporación” programs of the Ministerio de Economía y Competitividad of Spain. D.I. thanks the Marie Curie Actions, within the Innovative Training Network-European Joint Doctorate in Theoretical Chemistry and Computational Modelling TCCM-ITN-EJD-642294, for financial support. Computational time from the Centro de Computación Científica (CCC) of Universidad Autónoma de Madrid is also gratefully acknowledged. C.E.C.-H. acknowledges funding from the National Science Foundation (Grant No. CHE-1800052).

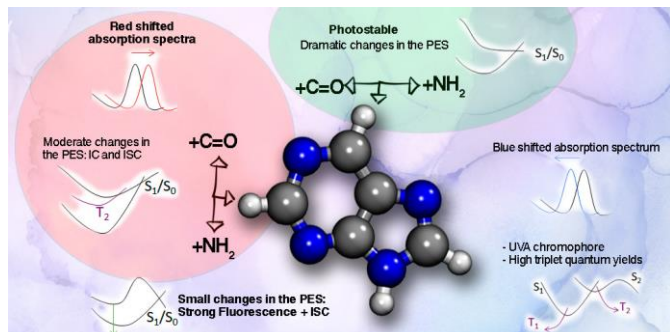
References

1. D. Gillingham, S. Geigle and O. Anatole von Lilienfeld, *Chemical Society Reviews*, 2016, **45**, 2637-2655.
2. E. Paleček and M. Bartošik, *Chemical Reviews*, 2012, **112**, 3427-3481.
3. Y. V. Suseela, N. Narayanaswamy, S. Pratihari and T. Govindaraju, *Chemical Society Reviews*, 2018, **47**, 1098-1131.
4. S. G. Trevino, N. Zhang, M. P. Elenko, A. Lupták and J. W. Szostak, *Proceedings of the National Academy of Sciences*, 2011, **108**, 13492-13497.
5. W. L. Ward, K. Plakos and V. J. DeRose, *Chemical Reviews*, 2014, **114**, 4318-4342.
6. Y. Zhao, F. Chen, Q. Li, L. Wang and C. Fan, *Chemical Reviews*, 2015, **115**, 12491-12545.
7. W. J. Schreier, P. Gilch and W. Zinth, *Annual Review of Physical Chemistry*, 2015, **66**, 497-519.
8. J. Cadet, S. Mouret, J.-L. Ravanat and T. Douki, *Photochemistry and Photobiology*, 2012, **88**, 1048-1065.
9. *From DNA Photolesions to Mutations, Skin Cancer and Cell Death*, RSC Publishing, Cambridge, UK, 2005.
10. J. S. Taylor, *Accounts of Chemical Research*, 1994, **27**, 76-82.
11. D. Markovitsi, *Photochemistry and Photobiology*, 2016, **92**, 45-51.
12. J. Cadet and T. Douki, *Photochemical & Photobiological Sciences*, 2018, **17**, 1816-1841.
13. J.-S. Taylor, *Science*, 2015, **347**, 824.
14. *Prebiotic chemistry and the molecular origins of life*, Physical Chemistry Chemical Physics Themed Collection. Royal Society of Chemistry, 2016.

15. A. C. Rios and Y. Tor, *Israel Journal of Chemistry*, 2013, **53**, 469-483.
16. C. E. Crespo-Hernández, B. Cohen, P. M. Hare and B. Kohler, *Chemical Reviews*, 2004, **104**, 1977-2020.
17. C. T. Middleton, K. de La Harpe, C. Su, Y. K. Law, C. E. Crespo-Hernández and B. Kohler, *Annual Review of Physical Chemistry*, 2009, **60**, 217-239.
18. T. Gustavsson, R. Improta and D. Markovitsi, *The Journal of Physical Chemistry Letters*, 2010, **1**, 2025-2030.
19. R. Improta, F. Santoro and L. Blancafort, *Chemical Reviews*, 2016, **116**, 3540-3593.
20. A. Giussani, J. Segarra-Martí, D. Roca-Sanjuán and M. Merchán, in *Photoinduced Phenomena in Nucleic Acids I. Topics in Current Chemistry*, ed. B. A. Barbatti M., Ullrich S., Springer, Cham, 2015, **355**, 57-97.
21. C. E. Crespo-Hernández, L. Martínez-Fernández, C. Rauer, C. Reichardt, S. Mai, M. Pollum, P. Marquetand, L. González and I. Corral, *Journal of the American Chemical Society*, 2015, **137**, 4368-4381.
22. L. Serrano-Andrés, M. Merchán and A. C. Borin, *Proceedings of the National Academy of Sciences of the United States of America*, 2006, **103**, 8691-8696.
23. M. Barbatti and H. Lischka, *Physical Chemistry Chemical Physics*, 2015, **17**, 15452-15459.
24. E. L. Rachofsky, J. B. A. Ross, M. Krauss and R. Osman, *The Journal of Physical Chemistry A*, 2001, **105**, 190-197.
25. K. A. Seefeld, C. Plützer, D. Löwenich, T. Häber, R. Linder, K. Kleinermanns, J. Tatchen and C. M. Marian, *Physical Chemistry Chemical Physics*, 2005, **7**, 3021-3026.
26. S. Perun, A. L. Sobolewski and W. Domcke, *Molecular Physics*, 2006, **104**, 1113-1121.
27. B. Mennucci, A. Toniolo and J. Tomasi, *The Journal of Physical Chemistry A*, 2001, **105**, 4749-4757.
28. C. Reichardt, C. Wen, R. A. Vogt and C. E. Crespo-Hernández, *Photochemical & Photobiological Sciences*, 2013, **12**, 1341-1350.
29. S. Lobsiger, S. Blaser, R. K. Sinha, H.-M. Frey and S. Leutwyler, *Nature Chemistry*, 2014, **6**, 989.
30. M. Barbatti and H. Lischka, *Journal of the American Chemical Society*, 2008, **130**, 6831-6839.
31. L. Blancafort, *Journal of the American Chemical Society*, 2006, **128**, 210-219.
32. I. Conti, M. Garavelli and G. Orlandi, *Journal of the American Chemical Society*, 2009, **131**, 16108-16118.
33. T. Gustavsson, N. Sarkar, I. Vayá, M. C. Jiménez, D. Markovitsi and R. Improta, *Photochemical & Photobiological Sciences*, 2013, **12**, 1375-1386.
34. S. Perun, A. L. Sobolewski and W. Domcke, *Journal of the American Chemical Society*, 2005, **127**, 6257-6265.
35. L. Serrano-Andrés, M. Merchán and A. C. Borin, *Chemistry – A European Journal*, 2006, **12**, 6559-6571.
36. E. Fabiano and W. Thiel, *The Journal of Physical Chemistry A*, 2008, **112**, 6859-6863.
37. J. P. Villabona-Monsalve, R. Noria, S. Matsika and J. Peón, *Journal of the American Chemical Society*, 2012, **134**, 7820-7829.
38. X. Guo, Z. Lan and Z. Cao, *Physical Chemistry Chemical Physics*, 2013, **15**, 10777-10782.
39. X. Guo, Y. Zhao and Z. Cao, *Physical Chemistry Chemical Physics*, 2014, **16**, 15381-15388.
40. X. Guo, H. Yuan, B. An, Q. Zhu and J. Zhang, *The Journal of Chemical Physics*, 2016, **144**, 154306.
41. S. Matsika, in *Photoinduced Phenomena in Nucleic Acids I. Topics in Current Chemistry*, ed. B. A. Barbatti M., Ullrich S., Springer, Cham, 2015, **355**, 209-243.
42. B. O. Roos, *In Ab initio Methods in Quantum Chemistry II Lawley, K. P. Ed.; Wiley: Chichester*, 1987.
43. W. J. Hehre, R. Ditchfield and J. A. Pople, *The Journal of Chemical Physics*, 1972, **56**, 2257-2261.
44. J. D. Dill and J. A. Pople, *The Journal of Chemical Physics*, 1975, **62**, 2921-2923.
45. J. Finley, P. Å. Malmqvist, B. O. Roos and L. Serrano-Andrés, *Chem. Phys. Lett.*, 1998, **288**, 299.
46. G. Ghigo, B. O. Roos and P.-Å. Malmqvist, *Chemical Physics Letters*, 2004, **396**, 142-149.
47. Y. Zhao and D. G. Truhlar, *Theoretical Chemistry Accounts*, 2008, **120**, 215-241.
48. A. Dreuw and M. Wormit, *Wiley Interdisciplinary Reviews: Computational Molecular Science*, 2015, **5**, 82-95.
49. T. H. Dunning, *The Journal of Chemical Physics*, 1989, **90**, 1007-1023.
50. A. Schäfer, C. Huber and R. Ahlrichs, *The Journal of Chemical Physics*, 1994, **100**, 5829-5835.
51. S. Miertuš, E. Scrocco and J. Tomasi, *Chemical Physics*, 1981, **55**, 117-129.
52. J. Tomasi, B. Mennucci and R. Cammi, *Chemical Reviews*, 2005, **105**, 2999-3094.
53. G. Scalmani, M. J. Frisch, B. Mennucci, J. Tomasi, R. Cammi and V. Barone, *The Journal of Chemical Physics*, 2006, **124**, 094107.
54. R. Improta, V. Barone, G. Scalmani and M. J. Frisch, *The Journal of Chemical Physics*, 2006, **125**, 054103.
55. R. Improta, G. Scalmani, M. J. Frisch and V. Barone, *The Journal of Chemical Physics*, 2007, **127**, 074504.
56. B. G. Levine, J. D. Coe and T. J. Martínez, *The Journal of Physical Chemistry B*, 2008, **112**, 405-413.
57. X. Gao, S. Bai, D. Fazzi, T. Niehaus, M. Barbatti and W. Thiel, *Journal of Chemical Theory and Computation*, 2017, **13**, 515-524.
58. F. Aquilante, J. Autschbach, R. K. Carlson, L. F. Chibotaru, M. G. Delcey, L. De Vico, I. Fdez. Galván, N. Ferré, L. M. Frutos, H. Agliardi, M. Garavelli, A. Giussani, C. E. Hoyer, G. Li Manni, H. Lischka, D. Ma, P. Å. Malmqvist, T. Müller, A. Nenov, M. Olivucci, T. B. Pedersen, D. Peng, F. Plasser, B. Pritchard, M. Reiher, I. Rivalta, I. Schapiro, J. Segarra-Martí, M. Stenrup, D. G. Truhlar, L. Ungur, A. Valentini, S. Vancoillie, V. Veryazov, V. P. Vysotskiy, O. Weingart, F. Zapata and R. Lindh, *Journal of Computational Chemistry*, 2016, **37**, 506-541.
59. TURBOMOLE V6.5, a development of University of Karlsruhe and Forschungszentrum Karlsruhe GmbH, 1989-2007, TURBOMOLE GmbH, since 2007; available from <http://www.turbomole.com>, 2013.
60. M. J. Frisch, et al *Gaussian 09, Revision A.1*, in, *Gaussian, Inc., Wallingford CT*, 2009.
61. B. Czochralska, H. Fritsche and D. Shugar, in *Zeitschrift für Naturforschung C1977*, vol. 32, p. 488.
62. S. F. Mason, *Journal of the Chemical Society (Resumed)*, 1954, 2071-2081.
63. E. Mburu and S. Matsika, *The Journal of Physical Chemistry A*, 2008, **112**, 12485-12491.
64. F. Seela, Y. Chen, U. Bindig and Z. Kazimierczuk, *Helvetica Chimica Acta*, 1994, **77**, 194-202.
65. D. Tuna, D. Lefrancois, Ł. Wolański, S. Gozem, I. Schapiro, T. Andruniów, A. Dreuw and M. Olivucci, *Journal of Chemical Theory and Computation*, 2015, **11**, 5758-5781.

66. S. Lobsiger, R. K. Sinha, M. Trachsel and S. Leutwyler, *The Journal of Chemical Physics*, 2011, **134**, 114307.

Table of contents:



Molding purine PES through functionalization: whilst purine C2-substitution maintains the features of the spectroscopic PES of the heterocycle, C6-functionalization reshapes its topography leading to photostable systems.
